Stability Analysis of Composite Cylindrical Shell Containing Rotating Fluid

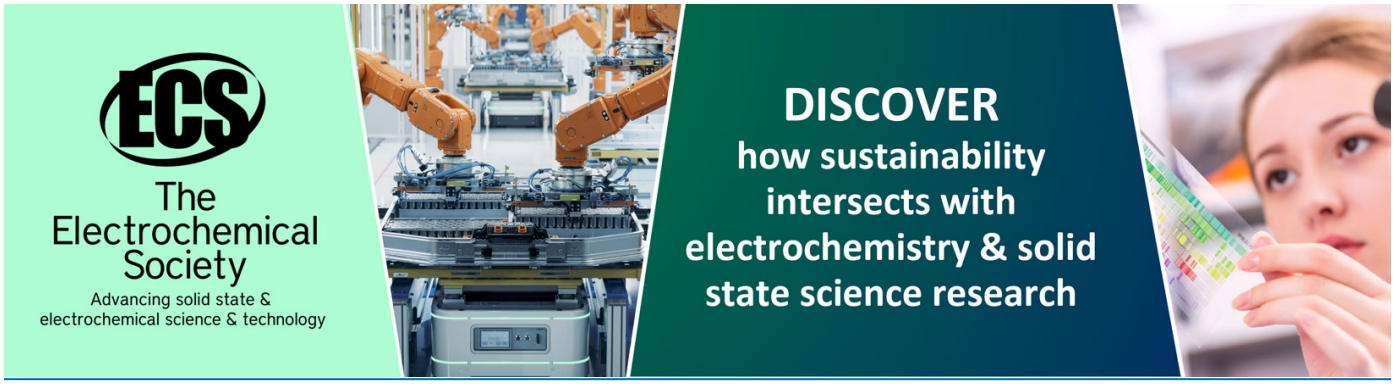

Journal of Physics: Conference Series **1945** (2021) 012034 doi:10.1088/1742-6596/1945/1/012034

Stability Analysis of Composite Cylindrical Shell Containing Rotating Fluid

S A Bochkarev [a] and S V Lekomtsev

Institute of Continuous Media Mechanics, Perm, Russian Federation

E-mail: [a] bochkarev@icmm.ru

Abstract. A semi-analytical finite element method is used to analyze the stability of composite cylindrical shells interacting with a rotating fluid inside them. A mathematical formulation of the problem of deformable structure dynamics is based on the variational principle of virtual displacements and classical shell theory. The behavior of an ideal compressible fluid is described within the framework of the potential theory. The validity of the obtained results is supported by comparing them with the known solutions. Numerical experiments were performed for two- and three-layer cross-ply shells made of boron-epoxy resin with different boundary conditions and geometrical dimensions. It is demonstrated that, for the examined configurations, an increase in the fibre angles leads to a significant increase in the critical rotation velocities of the fluid, regardless of the conditions for fixing the edges of a thin-walled structure.

1. Introduction

It is common knowledge [1–2] that in the process of industrial operation thin-walled elements of engineering structures can interact with liquid or gaseous medium. In some cases such medium is in a quiescent state, in others it flows inside the body or around it on the outside. In this case, either the axial or tangential velocity components or both simultaneously can be other than zero. The rotation of the fluid, as well as its axial flow, has a destabilizing effect on the structure, which at significant values of the angular velocity lose stability. Despite this fact, the number of publications, studying the effect of fluid rotation on the hydroelastic stability boundary, is limited. Analysis of the influence of rotating fluid or combined flow (rotation with axial flow) on the dynamic behavior of single and coaxial infinite shells, as well as shells of finite length, is carried out in papers [3–17]. In recent works, one of the ways to improve the critical parameters of systems is to use modern composite materials. Only a few publications [14,17] have focused on studying the influence of physical and mechanical parameters of shells made of functionally graded or piezoelectric materials on the critical velocities of fluid rotation. The analysis of properties of layered composite materials with different fiber angles is performed in [18–23] for a quiescent fluid completely filling the shell. Thus far, the effect of the properties of the layered composite on the hydroelastic stability boundary has not been adequately investigated and is the purpose of the present work.

2. Statement of the problem and constitutive relations

Let us consider an elastic cylindrical shell of length L, radius R and thickness h (figure 1). Inside the shell there is a perfect compressible fluid, which rotates with angular velocity Ω. The thin-walled structure is made of a unidirectional material (boron-epoxy resin AVCO 5505 [24]) whose layers are oriented at the angles of $+\alpha$ and $-\alpha$ relative to the meridional coordinate (cross-ply composite). We consider layered composite packages consisting of two $[\alpha, -\alpha]$ or three $[\alpha, 0°, -\alpha]$ layers. It is required to analyze the effect of the fiber angle α on the hydroelastic stability boundary of shells for different boundary conditions and geometric dimensions.

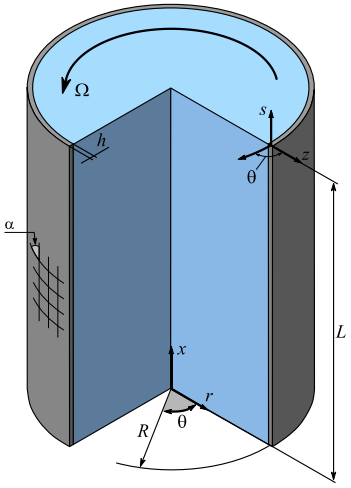

Figure1. Computational scheme.

To describe the motion of a rotating fluid in the region V_f, we introduce a perturbation velocity potential ϕ, which in the cylindrical coordinate system (r,θ,x) at small perturbations , is described by the wave equation [1]

$$\nabla^2\phi-\frac{1}{c^2}\frac{\partial^2\phi}{\partial t^2}=\frac{2\Omega}{c^2}\frac{\partial^2\phi}{\partial\theta\partial t}+\frac{\Omega^2}{c^2}\left(\frac{\partial^2\phi}{\partial\theta^2}-r\frac{\partial\phi}{\partial r}\right), \tag{1}$$

where c is the speed of sound in a liquid.

The fluid pressure P_f on the wetted surface of the elastic structure $S_\sigma=S_f\cap S_s$ is calculated using the linearized Bernoulli's formula

$$P_f=-\rho_f\left(\frac{\partial\phi}{\partial t}+\Omega\frac{\partial\phi}{\partial\theta}\right). \tag{2}$$

Here ρ_f is the specific density of liquid; S_f, S_s are the surfaces that bound fluid and shell regions, respectively. On the fluid-structure interface, the impermeability condition is prescribed

$$\frac{\partial\phi}{\partial n}=\frac{\partial w}{\partial t}+\Omega\frac{\partial w}{\partial\theta}, \tag{3}$$

where n is the normal to the surface, w is the normal component of the vector of shell displacements.

The perturbation velocity potential obeys the following boundary conditions

$$x=0:\ \frac{\partial\phi}{\partial x}=0,\qquad x=L:\ \phi=0. \tag{4}$$

The application of the Bubnov – Galerkin method to the partial differential equation for the perturbation velocity potential (1) with boundary conditions (3–4) allows us to obtain the following integral relation [4]:

$$\begin{aligned}&\sum_{l=1}^{m_f}\left\{\int_{V_f}\left[(\nabla F_l)^{\mathrm{T}}\nabla F_k+\frac{\Omega^2}{c^2}\left(\frac{\partial^2F_l}{\partial\theta^2}F_k-r\frac{\partial F_l}{\partial r}F_k\right)\right]\mathrm{d}V\ \phi_{al}\right\}+\sum_{l=1}^{m_f}\int_{V_f}\frac{2\Omega}{c^2}\frac{\partial F_l}{\partial\theta}F_k\mathrm{d}V\ \dot\phi_{al}\\&+\sum_{l=1}^{m_f}\int_{V_f}\frac{F_lF_k}{c^2}\mathrm{d}V\ \ddot\phi_{al}-\sum_{i=1}^{m_s}\left\{\int_{S_\sigma}N_i^wF_k\mathrm{d}S\ \dot w_{ai}+\int_{S_\sigma}\Omega\frac{\partial N_i^w}{\partial\theta}F_k\mathrm{d}S\ w_{ai}\right\}=0,\quad k=\overline{1,m_f}.\end{aligned} \tag{5}$$

Here: m_f, m_s are the number of unknowns (number of nodal values) in the fluid V_f and shell V_s regions; ϕ_{al}, w_{ap} are the coefficients to be determined (nodal values of perturbation velocity potential of the fluid and shell displacements); F, N^w are the known analytical functions (shape functions for the perturbation velocity potential and normal component of the shell displacement vector).

The shell is considered within the framework of the classical theory, which relies on the Kirchhoff – Love hypothesis. The vector components of deformation of the median surface, torsion and curvature changes in the coordinate system (s,θ,z) can be written as follows [25]:

$$\begin{aligned} &\varepsilon_1=\frac{\partial u}{\partial s},\quad \varepsilon_2=\frac{1}{R}\left(\frac{\partial v}{\partial\theta}+w\right),\quad \varepsilon_{12}=\frac{1}{R}\frac{\partial u}{\partial\theta}+\frac{\partial v}{\partial s},\\ &\kappa_1=-\frac{\partial^2 w}{\partial s^2},\quad \kappa_2=\frac{1}{R^2}\left(\frac{\partial v}{\partial\theta}-\frac{\partial^2 w}{\partial\theta^2}\right),\quad \kappa_{12}=\frac{1}{R}\left(\frac{\partial v}{\partial s}-\frac{\partial^2 w}{\partial s\partial\theta}\right). \end{aligned} \tag{6}$$

Here *u* and *v* are the meridional and circumferential components of the displacement vector of the shell.

The physical relationships that link the vector of generalized forces and moments $\boldsymbol{T}=\{T_{11},T_{22},T_{12},M_{11},M_{22},M_{12}\}^{\mathrm{T}}$ with the vector of generalized strains $\boldsymbol{\varepsilon}=\{\varepsilon_1,\varepsilon_2,\varepsilon_{12},\kappa_1,\kappa_2,2\kappa_{12}\}^{\mathrm{T}}$, are written in the matrix form as

$$\boldsymbol{T}=\mathbf{D}\boldsymbol{\varepsilon}=\begin{bmatrix}\bar{\mathbf{A}} & \bar{\mathbf{B}}\\ \bar{\mathbf{B}} & \bar{\mathbf{C}}\end{bmatrix}\boldsymbol{\varepsilon},\quad \left(\bar{a}_{ij},\bar{b}_{ij},\bar{c}_{ij}\right)=\int_h\left(1,z,z^2\right)\bar{Q}_{ij}dz,\quad (i,j=1,2,3), \tag{7}$$

where $\bar{Q}_{ij}$ are the components of the reduced matrix, which takes into account changes in the properties of the unidirectional material in the case when the local coordinate system is rotated by an angle α [26]. The elastic properties of the unidirectional material in the natural coordinates are determined in a known manner in terms of the elastic moduli E_1, E_2, Poisson's ratio ν_{12}, and shear modulus G_{12}.

A mathematical formulation of the problem of shell dynamics is based on the principle of virtual displacements, which, using the expression for the hydrodynamic pressure (2), can be written in the matrix form as

$$\int_{S_s}\delta\boldsymbol{\varepsilon}^{\mathrm{T}}\boldsymbol{T}\mathrm{d}S+\int_{S_s}\delta\boldsymbol{d}^{\mathrm{T}}\rho_0\ddot{\boldsymbol{d}}\mathrm{d}S-\int_{S_s}\delta\boldsymbol{d}^{\mathrm{T}}\boldsymbol{P}\mathrm{d}S=0. \tag{8}$$

Here $\boldsymbol{d}$, $\boldsymbol{P}=\{0,\,0,\,P_f\}$ are the vectors of displacements and surface loads, respectively, $\rho_0=\int_h\rho_s dz$, ρ_s is the specific density of the shell material.

3. Numerical implementation

Numerical implementation of the problem in the above mathematical formulation was performed using a semi-analytical finite element method [27], which is based on the representation of the solution as a Fourier series in the circular coordinate θ

$$\begin{aligned} &u=\sum\nolimits_{j=0}^{\infty}\hat{u}_j\cos j\theta+\sum\nolimits_{j=0}^{\infty}\breve{u}_j\sin j\theta,\quad v=\sum\nolimits_{j=0}^{\infty}\hat{v}_j\sin j\theta-\sum\nolimits_{j=0}^{\infty}\breve{v}_j\cos j\theta,\\ &w=\sum\nolimits_{j=0}^{\infty}\hat{w}_j\cos j\theta+\sum\nolimits_{j=0}^{\infty}\breve{w}_j\sin j\theta,\quad \phi_a=\sum\nolimits_{j=0}^{\infty}\hat{\phi}_j\cos j\theta+\sum\nolimits_{j=0}^{\infty}\breve{\phi}_j\sin j\theta. \end{aligned} \tag{9}$$

Here *j* is the number of harmonic.

Expressing the symmetric and antisymmetric unknowns in (9) in terms of the nodal displacements, we obtain the following expression for the finite elements of the shell and fluid

$$\boldsymbol{U}=\{u,v,w\}^{\mathrm{T}}=\mathbf{N}\boldsymbol{d}_e=\left[\hat{\mathbf{N}}\breve{\mathbf{N}}\right]\left\{\hat{\boldsymbol{d}}_e\breve{\boldsymbol{d}}_e\right\}^{\mathrm{T}},\quad \boldsymbol{\phi}_a=\mathbf{F}\boldsymbol{\phi}_e=\left[\hat{\mathbf{F}}\breve{\mathbf{F}}\right]\left\{\hat{\boldsymbol{\phi}}_e\breve{\boldsymbol{\phi}}_e\right\}^{\mathrm{T}}. \tag{10}$$

Here **N** and **F** are the matrices of shape functions, $\boldsymbol{d}_e$ and $\boldsymbol{\phi}_e$ are the vectors of nodal displacements. For the shell, we used the so-called high-precision finite element in the form of a truncated cone, in which the displacements are approximated by the Hermite polynomials of different degrees [28]. For the fluid, we used a triangular finite element with a linear approximation of the perturbation velocity potential

$$\begin{gathered}\widehat{u}_j = \sum_{i=1}^{2}\left(N_{2(i-1)+1}\widehat{u}_{ji} + N_{2(i-1)+2}\frac{\partial\widehat{u}_{ji}}{\partial s}\right),\ \widehat{v}_j = \sum_{i=1}^{2}\left(N_{2(i-1)+1}\widehat{v}_{ji} + N_{2(i-1)+2}\frac{\partial\widehat{v}_{ji}}{\partial s}\right)\\ \widehat{w}_j = \sum_{i=1}^{2}\left(H_{2(i-1)+1}\widehat{w}_{ji} + H_{2(i-1)+2}\frac{\partial\widehat{w}_{ji}}{\partial s} + H_{2(i-1)+3}\frac{\partial^2\widehat{w}_{ji}}{\partial s^2} + H_{2(i-1)+4}\frac{\partial^3\widehat{w}_{ji}}{\partial s^3}\right),\ \widehat{\phi}_j = \sum_{i=1}^{3}F_i\widehat{\phi}_{ji}.\end{gathered} \tag{11}$$

In view of (10), the relationship between the strain vector $\boldsymbol{\varepsilon}$ and the vector of nodal unknowns of the shell finite element $\boldsymbol{d}_e$ is given as

$$\boldsymbol{\varepsilon} = \mathbf{B}\boldsymbol{d}_e. \tag{12}$$

Substituting the value for pressure as defined in (2) into equation (8) and using the standard procedures of the finite element method with account of (10–12), we obtain the following matrix relation

$$\mathbf{K}_s\boldsymbol{d} + \mathbf{M}_s\ddot{\boldsymbol{d}} + \rho_f\mathbf{C}_{sf}^{\mathrm{T}}\dot{\boldsymbol{\phi}}_a + \rho_f\mathbf{A}_{sf}^{\omega}\boldsymbol{\phi}_a = 0, \tag{13}$$

where

$$\mathbf{K}_s = \sum_{m_s}\int_{S_s}\mathbf{B}^{\mathrm{T}}\mathbf{D}\mathbf{B}\mathrm{d}S,\ \mathbf{M}_s = \sum_{m_s}\int_{S_s}\mathbf{N}^{\mathrm{T}}\rho_0\mathbf{N}\mathrm{d}S,\ \mathbf{A}_{sf}^{\omega} = \sum_{m_s}\int_{S_\sigma}\Omega\mathbf{N}_w^{\mathrm{T}}\frac{\partial\mathbf{F}}{\partial\theta}\mathrm{d}S,\ \mathbf{C}_{sf} = \sum_{m_s}\int_{S_\sigma}\mathbf{N}_w^{\mathrm{T}}\mathbf{F}\mathrm{d}S\ .$$

Equation (5), taking into account expressions (10–11), can be written in the matrix form as follows:

$$\left(\mathbf{K}_f + \mathbf{K}_f^{\omega}\right)\boldsymbol{\phi}_a + \mathbf{M}_f\ddot{\boldsymbol{\phi}}_a - \mathbf{C}_f^{\omega}\dot{\boldsymbol{\phi}}_a - \mathbf{C}_{sf}\dot{\boldsymbol{w}}_a - \mathbf{A}_{fs}^{\omega}\boldsymbol{w}_a = 0, \tag{14}$$

where

$$\begin{gathered}\mathbf{K}_f = \sum_{m_f}\int_{V_f}\left(\nabla\mathbf{F}\right)^{\mathrm{T}}\nabla\mathbf{F}\mathrm{d}V,\ \mathbf{M}_f = \sum_{m_f}\int_{V_f}\frac{\mathbf{F}^{\mathrm{T}}\mathbf{F}}{c^2}\mathrm{d}V,\ \mathbf{C}_f^{\omega} = -\sum_{m_f}\int_{V_f}\frac{2\Omega}{c^2}\frac{\partial\mathbf{F}^{\mathrm{T}}}{\partial\theta}\mathbf{F}\mathrm{d}V,\\ \mathbf{K}_f^{\omega} = \sum_{m_f}\int_{V_f}\frac{\Omega^2}{c^2}\left[\frac{\partial^2\mathbf{F}^{\mathrm{T}}}{\partial\theta^2}\mathbf{F} - r\frac{\partial\mathbf{F}^{\mathrm{T}}}{\partial r}\mathbf{F}\right]\mathrm{d}V,\ \mathbf{A}_{fs}^{\omega} = \sum_{m_s}\int_{S_\sigma}\Omega\frac{\partial\mathbf{N}_w^{\mathrm{T}}}{\partial\theta}\mathbf{F}\mathrm{d}S.\end{gathered}$$

Thus, the study of stability of the shell, inside which the liquid rotates, is reduced to solving simultaneously the two systems of equations (13) and (14)

$$\left(\mathbf{K}+\mathbf{A}\right)\left\{\boldsymbol{d}\ \ \boldsymbol{\phi}_a\right\}^{\mathrm{T}} + \mathbf{M}\left\{\ddot{\boldsymbol{d}}\ \ \ddot{\boldsymbol{\phi}}_a\right\}^{\mathrm{T}} + \mathbf{C}\left\{\dot{\boldsymbol{d}}\ \ \dot{\boldsymbol{\phi}}_a\right\}^{\mathrm{T}} = 0, \tag{15}$$

where

$$\begin{gathered}\mathbf{K} = \mathrm{diag}\left\{\mathbf{K}_s\ -\rho_f\left(\mathbf{K}_f + \mathbf{K}_f^{\omega}\right)\right\},\\ \mathbf{M} = \mathrm{diag}\left\{\mathbf{M}_s\ -\rho_f\mathbf{M}_f\right\},\end{gathered}\qquad \mathbf{C} = \rho_f\begin{bmatrix}0 & \mathbf{C}_{sf}^{\mathrm{T}}\\ \mathbf{C}_{sf} & \mathbf{C}_f^{\omega}\end{bmatrix},\ \mathbf{A} = \rho_f\begin{bmatrix}0 & \mathbf{A}_{sf}^{\omega}\\ \mathbf{A}_{fs}^{\omega} & 0\end{bmatrix}.$$

Representing the perturbed motion of the shell and fluid as

$$\boldsymbol{d} = \boldsymbol{q}\exp(\mathrm{i}\lambda t),\quad \boldsymbol{\phi}_a = \boldsymbol{\phi}\exp(\mathrm{i}\lambda t),\quad \mathrm{i} = \sqrt{-1},\quad \lambda = \lambda_1 + \mathrm{i}\lambda_2,$$

where $\boldsymbol{q}, \boldsymbol{\phi}$ is some function of coordinates, λ is the characteristic quantity, we finally arrive at

$$\left(\mathbf{K} - \lambda^2\mathbf{M} + \mathrm{i}\lambda\mathbf{C} + \mathbf{A}\right)\left\{\boldsymbol{q}\ \ \boldsymbol{\phi}\right\}^{\mathrm{T}} = 0. \tag{16}$$

The solution of the problem is reduced to the evaluation and analysis of complex eigenvalues λ of the system (16). For these purposes, we use an algorithm, which is based on the Muller method [29].

Taking into account the selected series expansion (9) and derivatives with respect to θ in the matrices $\mathbf{A}_f^{\omega}$ and $\mathbf{A}_s^{\omega}$, the symmetric unknowns of the shell are linked to the asymmetric fluid variables and symmetric unknowns of the fluid – to the asymmetric variables of the shell. In the matrix $\mathbf{C}_f^{\omega}$, linking of the symmetric to the asymmetric fluid unknowns is performed. Note that in this case matrices **A** and $\mathbf{C}_f^{\omega}$ are asymmetric.

4. Examples of numerical implementation

The calculations were carried out for several variants of the boundary conditions specified at the edges of the shell (R = 1 m, h = 0.01 m): F corresponds to a free edge; S is a simply supported structure ($v = w = 0$); C is clamping $(u = v = w = \partial w/\partial s = 0)$. The properties of unidirectional material are taken as follows [24]: $E_1 = 206.9$ GPa, $E_2 = 18.62$ GPa, $\nu_{12} = 0.28$, $G_{12} = 4.48$ GPa.

4.1. Algorithm verification

The verification of the developed finite-element algorithm was performed in the context of two example problems. Table 1 shows the natural frequencies Re(λ) (Hz) of vibrations of an empty cylindrical shell rigidly clamped at both edges. The frequencies were obtained for different values of the angle α and laying patterns of the composite material. The disagreement with the results of work [24], which are also presented in the table, does not exceed 2.5%.

The next example is the hydroelastic stability of an isotropic shell. Figure 2 shows the evolution of real Re(ω) and imaginary Im(ω) parts of the dimensionless eigenvalue $\omega = R\lambda\xi$ as a function of the dimensionless angular velocity $\Omega^* = R\Omega\xi$ of the fluid for two lower frequencies $(\xi = \left[\rho_m\left(1-\nu_{12}^2\right)/E_1\right]^{1/2})$. Here, m denotes the number of half-waves in the meridional direction. The rotation of the fluid causes the frequency to split into two values, which corresponds to the appearance of a forward and reverse wave. An increase in the rotation speed of the liquid leads to an increase in the eigenvalues, corresponding to the forward waves (depicted in the figure by solid lines), and a decrease in the eigenvalues, corresponding to the reverse waves (dashed lines). At the angular velocity Ω_0^*, the real part of reverse wave of the 1st mode is equal to zero and begins to increase with further increase in the angular velocity. The real parts of both waves of the first mode coalesce at the angular velocity Ω_F^*.

Table 1. Comparison of natural vibration frequencies (Hz) of empty layered cylindrical shells rigidly clamped at both edges.

α	Two layers [α, −α]		Three layers [α, 0°, −α]	
	Ref. [24]	computation	Ref. [24]	computation
0°	261.41	261.13	261.41	261.13
15°	351.75	351.01	337.63	337.03
30°	369.56	366.39	397.58	395.95
45°	340.95	332.64	446.24	443.78
60°	359.36	352.56	487.64	485.69
75°	382.24	380.13	465.54	464.63
90°	333.43	332.53	370.71	370.09

This is accompanied by the appearance of the equal imaginary parts opposite in sign (dashed line), which characterizes the onset of instability in the form of coupled-mode flutter. In the case of fluid rotation, this type of stability loss does not depend on the type of boundary conditions prescribed at the edges of the shell, in contrast to the fluid flow having only an axial component. The figure shows the

results of [17], which also demonstrate good agreement between the solutions obtained by different methods.

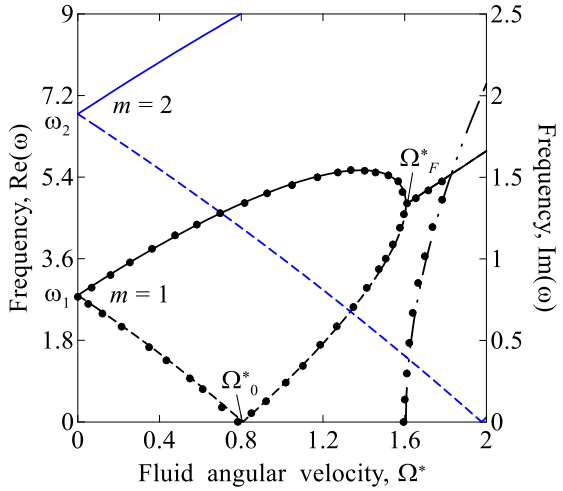

Figure 2. The dependence of the real Re(ω) and imaginary Im(ω) parts of dimensionless natural frequencies on the dimensionless speed of fluid rotation Ω* for the shell, simply supported at both edges.

4.2. Study of hydro-elastic stability

Figure 3 shows the critical angular velocity of the fluid rotation Ω as a function of the fiber angle α obtained for two- and three-layered shell (*L*/*R* = 2) for different boundary conditions. Here, symbols denote changes in the vibration modes as a function of minimum angular velocity of the fluid, and figures indicate the number of half-waves in the circumferential direction *j*. For both reinforcement packages, there is a tendency to a growth of the critical angular velocities of fluids with increasing fiber angle α up to a threshold value, after which a slight decrease is observed. For shells with any type of boundary conditions the growth is almost two-fold for a two-layer package, and even greater for a three-layer package.

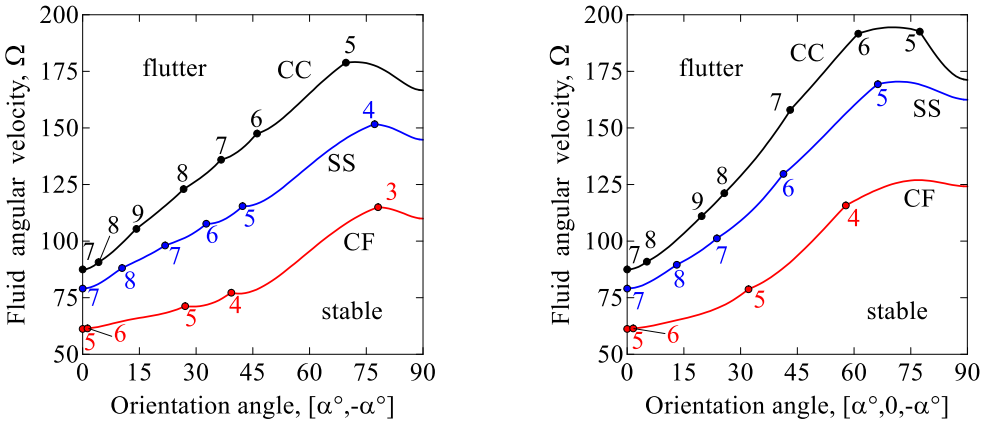

Figure 3. Dependences of the critical angular velocity of the fluid Ω (rad/s) on the fiber angle α of the layered cylindrical shell with different boundary conditions and reinforcement package (*L*/*R* = 2).

Figure 4 shows similar dependencies, but for a longer shell (*L*/*R* = 10). Qualitatively, the curves show the same behavior with the following exception. First, the transitions to different vibration modes with a change in the minimum angular velocity are more pronounced. Second, in the case of certain boundary conditions, there is a range of angles, in which the stability boundary decreases even by comparison with the non-oriented unidirectional material (α = 0°). For example, for a cantilevered structure this

range is between 32 and 46 degrees, while for a simply supported structure it is between 26 and 32 degrees.

As for other aspects, the results presented in Figures 3 and 4 show the traditional dynamic behavior: a decrease in the critical velocities is observed for longer shells; the boundary conditions, which favor stiffening of the system, are also responsible for the growth of the angular velocities of the fluid.

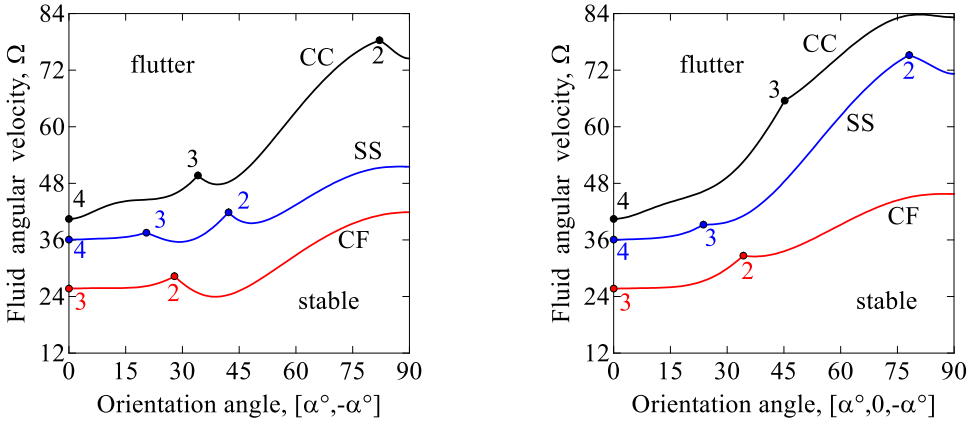

Figure 4. Dependences of the critical angular velocity of the fluid Ω (rad/s) on the fiber angle α of the layered cylindrical shell with different boundary conditions and reinforcement packages (L/R = 10).

5. Conclusions

The results of numerical calculations presented in this paper demonstrate that for the examined configuration and invariable geometric dimensions it is possible to achieve a significant increase in the parameter leading to the loss of stability by selecting an appropriate scheme of reinforcement and fiber angle for the layered composite material.

Acknowledgments

The study was made in the framework of the government order; state registration number of theme AAAA-A19-119021490136-7.

References

[1] Ilgamov M A 1969 *Oscillations of Elastic Shells Containing Liquid and Gas* (Moscow: Nauka)
[2] Païdoussis M P 2016 *Fluid-Structure Interactions: Slender Structures and Axial Flow* (London: Academic Press) vol 2
[3] Srinivasan A V 1971 *AIAA J* **9** 394
[4] David T S and Srinivasan A V 1974 *AIAA J* **12** 1631
[5] Chen T L C and Bert C W 1977 *Nucl. Eng. Des.* **42** 247
[6] Chen T L C and Bert C W 1977 *J. Appl. Mech.* **44** 112
[7] Vorob'ev Yu S and Detistov S I 1985 *Int. Appl. Mech.* 21 657.
[8] Bochkarev S A and Matveenko V P 2011 *Comput. Struct.* **89** 571.
[9] Bochkarev S A and Matveenko V P 2012 *Mech. Solids* **47** 560
[10] Bochkarev S A and Matveenko V P 2013 *Int. J. Mech. Sci.* **68** 258
[11] Bochkarev S A and Matveenko V P 2013 *J. Sound Vib.* **332** 4210
[12] Bochkarev S A and Matveenko V P 2015 *J. Vib. Acous.* **137** 021001
[13] Bochkarev S A and Matveenko V P 2015 *Int. J. Struct. Stab. Dyn.* **15** 1450071
[14] Ning W-B, Zhang J-G and Chen W-D 2016 *Acta Mech.* **227** 2157
[15] Ning W-B, Zhong M, Hu G and Luo Y 2017 *Int. J. Mech. Sci.* **134** 136
[16] Pour H R, Arani A G and Sheikhzadeh G A 2017 *Steel Compos. Struct.* **23** 691
[17] Arani A G, Karimi M S and Bidgoli M R 2017 *Polym. Compos.* **38** E577
[18] Xi Z C, Yam L H and Leung T P 1997 *J. Acoust. Soc. Am.* **101** 909

[19] Xi Z C, Yam L H and Leung T P 1997 *Compos. Pt. B-Eng.* **28** 359
[20] Thinh T I and Nguyen M C 2016 *Appl. Math. Model.* **40** 9286
[21] Izyan M D N, Aziz ZA and Viswanathan K K 2018 *Compos. Struct.* **193** 189
[22] Izyan M D N, Aziz Z A, Ghostine R, Lee J H and Viswanathan K K 2019 *Int. J. Pres. Ves. Pip.* **170** 73
[23] Izyan M D N and Viswanathan K K 2019 *PLoS ONE* **14** e0219089
[24] Sheinman I and Greif S 1984 *J. Compos. Mat.* **18** 200
[25] Biderman V L 1977 *Mechanics of Thin-walled Structures* (Moscow: Mashinostroenie)
[26] Alfutov N A, Zinov'ev P A and Popov B G 1984 *Analysis of Multilayer Plates and Shells of Composite Materials* (Moscow: Mashinosiroenie)
[27] Zienkiewicz O C 1972 *Finite Element Method in Engineering Science* (New York: McGraw-Hill)
[28] Shivakumar K N and Krishna Murty A V 1978 *J. Sound Vib*. **58** 311
[29] Matveenko V P, Sevodin M A and Sevodina N V 2014 *Comp. Cont. Mech.* **7** 331